Imprints of wave climate and mean sea level variations in the dynamics of a coastal spit over the last 250 years: Cap Ferret, SW France

Alphonse Nahon, Déborah Idier, Nadia Senechal, Hugues Féniès, Cyril Mallet, Julie Mugica

Earth Surface Processes and Landforms

Imprints of wave climate and mean sea level variations in the dynamics of a coastal spit over the last 250 years: Cap Ferret, SW France

Journal:	*Earth Surface Processes and Landforms*
Manuscript ID	ESP-18-0356.R3
Wiley - Manuscript type:	Research Article
Date Submitted by the Author:	n/a
Complete List of Authors:	Nahon, Alphonse; Université de Bordeaux, UMR CNRS 5805 EPOC; Bureau de Recherches Geologiques et Minieres, Idier, Déborah; BRGM - French Geological Survey, DRP Sénéchal, Nadia; University of Bordeaux, UMR EPOC Féniès, Hugues; ENSEGID, Géoressources et Environnement Mallet, Cyril; BRGM - French Geological Survey, Aquitaine agency Mugica, Julie; BRGM - French Geological Survey, Aquitaine agency
Keywords:	Barrier systems, Tidal inlet, Sea level rise, NAO, Dalton Minimum

Imprints of wave climate and mean sea level variations in the dynamics of a coastal spit over the last 250 years: Cap Ferret, SW France

Alphonse Nahon[1,2], Déborah Idier[3], Nadia Sénéchal[1], Hugues Féniès[4], Cyril Mallet[1] and Julie Mugica[1]

[1] University of Bordeaux, UMR EPOC, Pessac, France.

[2] BRGM – French Geological Survey, Nouvelle-Aquitaine agency, Pessac, France.

[3] BRGM – French Geological Survey, Risks and prevention department, Orléans, France.

[4] ENSEGID, Pessac, France.

Corresponding author: Alphonse Nahon (alphonse.nahon@u-bordeaux.fr)

Key words:

Barrier systems; Tidal inlet; Sea level rise; Climate; NAO; Dalton Minimum.

Abstract

In coastal areas, sea level rise (SLR) and changing wave climates are expected to be the main oceanic drivers of shoreline adjustments. These drivers have been shown to vary on a wide spectrum of spatial and temporal scales. Nonetheless, a general rule about how this variability impacts global shorelines remains to be articulated. Here, we discussed the impacts of wave climate changes and SLR on the evolution of a barrier-spit – inlet system over the last 250 years. The distal end of the Cap Ferret barrier-spit, SW France, has undergone large-scale oscillations that were well correlated with variations of the decadal average of the winter North Atlantic Oscillation (NAO) index. The local wave climate hindcast supports that increased alongshore wave energy fluxes associated with the positive phase of the NAO were responsible for the updrift retreat of the spit. In another case, the spit has elongated downdrift when waves were less energetic and more shore normal, as during the negative phase of the NAO. In addition, lower rates of SLR appeared necessary for the spit to develop, as higher rates of SLR very likely forced the adjacent inlet to enlarge, at the expense of the spit. These results should help to predict and detect coastal adjustments driven by climate change and variability.

Introduction

Slower eustatic sea level rise (SLR) over the last 6 *ka* has allowed the formation of barrier spits at the entrance of many of the world's estuaries and bays (Davis, 2013). Growing barriers would then create bar-built estuaries or coastal lagoons where rich ecosystems have developed. Provided that such sheltered areas remained open to the sea, they have become attractive for human activities. This has added an economic dimension to their ecological value and role (Newton et al., 2014). Such factors are among the many reasons that continue to motivate multidisciplinary studies to improve our understanding of barrier spit dynamics and their interactions with estuary and lagoon entrances.

Where sediments are abundant, it is recognised that sort of a competition between wave-driven alongshore sediment transport (LST) and estuarine (fresh and saltwater) flows, controls the existence of spits as it does for inlets (FitzGerald et al., 2015; Hayes, 1979; Nichols and Allen, 1981). From the spit perspective, LST generally plays a constructive role while flows favour inlets (Kraus, 1998; Kraus and Seabergh, 2002). Inlet (cross-section) stability can be rated as good, fair or poor based on the ratio of the spring tidal prism by the total littoral drift (Bruun, 1978). Larger freshwater inputs ultimately favour inlet stability as confirmed by numerical modelling (Zhou et al., 2014). These forces vary as waves, sea level and rainfalls change with seasons and climate shifts. In mixed-energy environments (Hayes, 1979), such variability can lead to noticeable changes of local morphology. Such changes may occur fortnightly, as it does for small systems (Fortunato et al., 2014), and at any larger timescale at which driving forces may change. For instance, if most barrier spits were able to build during periods

with relatively low rates of sea-level rise (SLR), questions remain about how they would respond to predicted higher rates of SLR and changing wave climate for the coming decades (Cazenave and Le Cozannet, 2014; Semedo et al., 2013).

There is indeed a persistent and immediate need to improve the prediction of climate change impacts on coastal systems worldwide (Wong et al., 2014). Main drivers include SLR, the alteration of rainfall and runoff and changing wave climates which are crucial for spits and inlets' evolution (Ranasinghe et al., 2012). In most coastal embayments, SLR leads to larger values of tidal prisms that force inlets to increase their cross-section (FitzGerald et al., 2008). In places with low continental sediment inputs, SLR would also create accommodation space in embayments that may become sediment sinks for the adjacent coasts (Ranasinghe et al., 2012). Where freshwater runoff contributes to maintain inlets, it may also cause adjacent spit retreat or progradation as rainfall respectively increases or diminishes (Ranasinghe et al., 2012). Finally, changing storm tracks, storm intensity and frequency are likely to modify coastal resilience (Masselink et al., 2016) and have a direct impact on the wave driven LST (Chowdhury and Behera, 2017; Splinter et al., 2012).

Along with natural climate variability, these drivers have already varied over a wide range of temporal and spatial scales. At inter-annual to decadal timescales, atmospheric teleconnection patterns, such as the North Atlantic Oscillation (NAO), and climatic cycles such as the El Niño Southern Oscillation (ENSO) over oceanic basins have remote effects on coastal environments (Barnard et al., 2011; Masselink et al., 2014; Wiggins et al., 2017). On longer timescales, the stratigraphic records of coastal barrier spits have also revealed the control exerted by sea level changes (Clemmensen

et al., 2001; Fruergaard et al., 2015) and major storm events (Fruergaard et al., 2013). This climate-driven variability can overlay the system internal cyclicity and play a part in rhythmic behaviours that are common along barrier coasts (Allard et al., 2008; Ridderinkhof et al., 2016). These cycles have substantial effects on shoreline dynamics. Nonetheless, due to limited number of detailed geomorphological datasets, on the longer term it is often unclear whether cyclicity is driven by the system intrinsic nature (i.e., autocyclic) or by external (climatic) factors (i.e., allocyclic).

On the other hand, global knowledge on climate variability and its effects is constantly growing. Coupled ocean-atmosphere numerical models help to describe processes underlying relationships between parameters of different nature as, for instance, sea level pressure, anomalous coldness and storm tracks (van der Schrier and Barkmeijer, 2005), solar irradiance and teleconnection patterns (Ineson et al., 2011) or teleconnection patterns and sea level (Calafat et al., 2012). Going back to interactions between barrier spits and inlets, recent studies address the impact of climate change through the application of process-based morphodynamic models to tidal embayments (Bruneau et al., 2011; Dissanayake et al., 2012; van Maanen et al., 2013; van der Wegen, 2013). Those studies primarily discuss the effects of SLR and describe the evolution of the sediment source-to-sink nature of inlets over time. Such growing understanding of both the dynamic nature of climate and of the processes changing the coastal landscape widens the spectrum of possibilities for interpreting documented coastal evolutions.

This study thrives on these possibilities to discuss the coherence between large-scale coastal changes and variable environmental conditions. The next section presents a

dataset with outstanding temporal coverage and resolution. It covers the morphological evolution of the Cap Ferret sand spit (SW France, Atlantic coast) over the last 250 years and contemporaneous environmental conditions. Then section 3 investigates the synchronisation of the apparent cyclical dynamic of the spit distal end with climatic shifts and sea level variations. Potential mechanisms underlying this synchronisation are subsequently discussed based on current understanding of barrier spits and tidal inlets morphodynamics, allowing to identify the dominant climatic drivers (section 4).

Materials and methods

Study area

The Cap Ferret is a baymouth spit bordered by the Bay of Biscay (Figure 1). It lies at the southern end of a 110 km long uninterrupted sandy beach bounded by the Gironde estuary to the north (Aubié and Tastet, 2000; Castelle et al., 2018; Figure 1b). The subaerial fraction of the spit accounts for the beach last twenty kilometres and is built upon a subtidal platform that dips into the Bay of Arcachon tidal inlet (Figure 1c). This inlet connects a 160 km^2 coastal lagoon to the Atlantic Ocean, the lagoon – inlet system being the vestige of the Leyre River estuary (Féniès and Lericolais, 2005). Around 3 *ka* ago the Cap Ferret started to build up on the estuary northern margin (Féniès et al., 2010), pushing the river mouth southward until it semi-enclosed the Bay of Arcachon. At present, water circulation between the lagoon and the ocean constricts the spit progradation. Twice a day between 260 and 490 Mm^3 of water flow in and out through the inlet, confirming that at any time tidal exchanges largely take over on freshwater inputs (Plus et al., 2009). Such high values of tidal prism (P) largely overcome the total

LST (M), estimated at 0.661 Mm^3 (Idier et al., 2013), so that this opening falls into the "good stability" category (P/M >> 150) of (Bruun, 1978) classification. Nonetheless, northwesterly dominant waves have deviated the estuary mouth some thirty kilometres downdrift in the past 3 *ka* (Féniès et al., 2010). Annual mean significant wave height is of 1.77 m (in 50 m water depth, according to Charles et al., 2012) and mean tidal range is of 2.7 m (twice the semidiurnal tidal component amplitude, measured on the ebb-delta's shield, by Senechal et al., 2013). This mixed-energy environment, as defined by Hayes (1979), has moulded an inlet with a transitional morphology (Hubbard et al., 1979). The inlet ebb-tidal delta is more developed than the flood-tidal shoals (Figure 1c). This disequilibrium reflects the ebb dominance confirmed by morphodynamic modelling (Cayocca, 2001). Model results further showed the role of the ebb-dominant tide in the breaching of new channels across the spit platform. Indeed, historical charts report various occurrences of the formation of a new channel across the platform. Over the last 300 years, newly opened channels have migrated southward and the detached shoals ultimately reached and merged to the inlet southern margin, in a movement that resembles the spit-platform breaching model of sediment by-passing of FitzGerald et al. (2001). The apparent cyclical nature of this process has led to the hypothesis of an 80-year autocyclic behaviour. According to charts, the inlet has been alternatively composed of one or two channels and Michel and Howa (1997) further interpreted the retreat of the subaerial fraction of the spit as a feedback from the breaching of new (secondary) channels. However, a thorough discussion of the role of variable environmental conditions is still lacking. The premises of such a discussion were given by Nahon et al. (2015). In this first analysis, it was noted that the autocyclic model fails

to predict a major spit progradation event. Instead, spit elongation was found synchronous with periods dominated by the negative phase of the NAO.

The present study builds upon Nahon et al. (2015) data to further infer on the role that climate and SLR may have played in inlet – spit interactions. Cap Ferret is well suited for this study because of 3 reasons: 1) updrift sandy beaches prevent from any sediment deficit; 2) it is backed up by a mature estuary where an elevated level of infilling makes tidal prism sensitive to mean sea level variations; 3) the first quantitatively valuable chart dates from 1768 and the evolution of the spit-inlet system can be reconstructed over the last 2.5 centuries.

Shoreline data

The geomorphological record encompasses the entire 19th and 20th centuries and consists of nautical charts and aerial photographs of the Bay of Arcachon's tidal inlet (Figures 2 to 4).

Charts were retrieved from Caspari (1872), Lapeyre (1925) and Bordeaux harbour authorities (PAB, 1985). All made appear 3 reference positions on charts (Figure 2): the still existing Cap Ferret's lighthouse and the church *Notre-Dame d'Arcachon*, both located north of the spit distal end, and a former semaphore on the southern margin. This later position was retrieved from the map of the Gironde department in 1888 (Figure 2a). These positions were used for georeferencing.

Clear and stable features along the spit were used to estimate the error on the charts before 1900. Preserved former spit-end positions and small bights on the lagoon side of the spit, indicate a distance error well below 200 m. Therefore, a +/- 200 m error bars

marks off the results to avoid any misinterpretation. Early 20th century charts also indicate a (still existing) semaphore located 1 km north of the 2014 shoreline. The root mean square error for the semaphore positions is 55 m and results are also shown with +/- 100 m error bars to account for possible shoreline misinterpretation at the time of the survey. The spit terminus was then defined as the southernmost position of the coastline represented on charts (Figure 3). These positions were orthogonally projected onto the axis defined by 2 of the reference positions used for georeferencing nautical charts (Figure 3).

Positions measured on charts from 1932 and 1936 presented a very good match with those on photographs from 1934 and 1946 respectively (Figure 4). Between 1934 and 2000, aerial photographs were used. They were georeferenced using the current road and pathway network and, at some point, World War II bunkers on top of the dunes. After 2000, 7 high resolution orthophotomaps were used. Georeferencing errors are lower than the shoreline photo-interpretation error that was estimated well below +/- 50 m. On photographs, the southernmost position of the interpreted shoreline (i.e. berm crest when perceptible, high-tide wrack line otherwise) was taken to measure the spit extension. Overall, 50 positions of the Cap Ferret distal end were retrieved since 1768 (24 on charts from 1768 to 1936, Figure 3; 26 on photographs from 1934 to 2014, Figure 4). These positions were used to trace the path of the spit distal-end. In the following, periods over which the spit advanced across the inlet were identified from this path. Still, it is a limited indicator of erosion or accretion patterns as it does not consider the behaviour of the spit in the direction perpendicular to the reference axis.

Bathymetric data

Shoreline data document north-south oscillations of the spit distal end, the last large-scale oscillation occurring between 1950 and 2014 (Figure 4). Over this period, bathymetric evolution of the adjacent inlet throat was quantified using soundings from years 1949, 1969, 1979, 2001 and 2014.

Over the years, along transect resolution increased from 100 m to 1 m and transect positioning and spacing (~200m) remained constant (Figure 5a). For each survey, transects have been interpolated into digital elevation models (DEMs); 50 m x 50 m surfaces were created using a nearest-neighbour interpolation (Figure 5b). Bottom elevation and volumetric changes were computed over a 12.74 km^2 overlapping surface between all 5 DEMs. Figure 5d presents the erosion-deposition patterns over the 65 years.

A distinction was made between shoals and channels using the -7 m NGF contour (NGF is the French vertical datum; locally Mean Sea Level is currently around +0.40 m NGF). This contour match well with shoals visible on contemporary Landsat 8 image (Figure 5c). For each date, 4 quantities were computed. The first 3 are the mean elevation and the shoal and channel volumes which are respectively the sand volume above -7 m NGF and water volume below -7 m NGF. As little to none information exists to estimate errors due the instrumental bias or vertical datum changes over time (others than the known and corrected ones), a fourth quantity, defined as the inlet throat *morphological amplitude* was calculated. It corresponds to the equal volumes of sand and water, respectively above and below the mean elevation of each DEM. In this way, this later quantity is free of any artificial variations. Results are summarised in Table 1.

Figure 5 (e-h) further presents the variation of the computed quantities with the identified periods of elongation and retreat of the spit-end.

Sea level data

To infer on the role of sea level variations in the evolutions depicted by cartographic and bathymetric data, the annual mean sea level (MSL) record from Brest tidal gauge (Figure 1) was retrieved from the permanent mean sea level observatory (Holgate et al., 2013); it is the nearest tidal gauge with an appropriate temporal coverage (Wöppelmann et al., 2008). Over the entire period the data is fitted to a 2nd order polynomial function which reveals the lowering of MSL during the first third of the 19th century (Figure 6, upper panel). Then over the 20th century, the data is both averaged and fitted to a polynomial function. The running mean over an 11-year-centred window is used to emphasise the significant decadal variability of the regional MSL. Then, fitting the record with 5th order polynomial function allows identifying a period of slower SLR around the second third of the 20th century (Figure 6, lower panel).

Table 2 further indicates average SLR rates over identified periods of spit growth and decay. Rates are computed as the linear trend in the overlapping sea level data. The overlap is defined by adding sea level data until preceding and following spit-end positions to the actual identified period (excepted for 1909 because of the important 20-year interval between positions). This lengthens the periods over which the trend is computed. When computed over the exact (shorter) intervals, differences between successive periods of growth and decay are more pronounced.

Wave climate data

To assess the impact from variations of wave-driven forces, the local wave climate during the last oscillation of the spit-end was characterized by means of a hindcast simulation, performed with the storm surge modelling system of Bertin et al. (2015). The model was extended to the whole North Atlantic Ocean and forced with wind fields originating from the NCEP/NCAR reanalysis (Kalnay et al., 1996), over the period 1949-2014. Hindcasted wave parameters were validated against measurements from a directional wave buoy moored in 54 m water depth, and located 15 km offshore the study site (CETMEF, n.d.). Between 2007 and 2014, 92602 measurements, representative of 5.3 years in record length, were compared to interpolated modelled parameters. For both modelled and measured parameters, the wave power (WP) is approximated with the linear wave theory (Svendsen, 2006; Eq. 1-2), as the wave energy (E) times the wave group velocity (c_g), after computing the phase velocity (c) using an iterative method to solve the dispersion relationship for calculating (in intermediate water depth) the wave number (k) associated with the peak angular frequency (ω).

Eq. 1: $$WP = Ec_g$$

Eq. 2: $$E = \frac{1}{8}\rho g\, Hs^2;\ c_g = c * \frac{1}{2}\left(1 + \frac{2kh}{\sinh 2kh}\right);\ c = \frac{\omega}{k}$$

The WP is then decomposed into cross-shore (WPx) and alongshore (WPy) energy flux, positive when landward and northward respectively. Table 3 summarizes the comparison outcomes for the significant wave height (Hs), the WP and mean wave

energy direction (wDir), computed with mean WPx and WPy. Modelled and observed parameters are in good agreements. Pearson linear correlation coefficient are equal to 0.93 and 0.80 for respectively WP and WPy and the modelled wave field only slightly underestimating the total WP by 2.4%. In terms of direction, wDir has an initial bias of 3.8º. After removing the bias, correlation between modelled and observed WPy is improved to 0.81 and the error on averaged WPy is minimal (1.7%). Low-pass filtered WP and WPy on Figure 7 further reveal the good performance of the model, as correlation coefficients grow to 0.99 and 0.95 for WP and WPy respectively.

North Atlantic Oscillation (NAO)

Over the entire period covered by geomorphological data, winter indices of the North Atlantic Oscillation (NAO) provide additional information about the environmental forcing. The NAO is the main atmospheric mode of variability over the North Atlantic basin in winter (Hurrell and Deser, 2009), and from December to March, its negative and positive phases have a demonstrated influence on ocean waves and sea level anomalies on Western Europe coastlines (Calafat et al., 2012; Dodet et al., 2010). Therefore, 3 different NAO indices were used as proxy for these environmental drivers. Indices of the winter NAO in the literature are either reconstructions based on a combination of instrumental and proxy data (Cook et al., 2002; Glueck and Stockton, 2001; Luterbacher et al., 1999; Ortega et al., 2015), indices computed from the difference of normalized sea level pressure between the Azores High and the Icelandic Low (Hurrell, 1995; Jones et al., 1997), or indices based on a principal component analysis of reconstructed sea level pressure fields over the North Atlantic Ocean

(Barnston and Livezey, 1987; Hurrell, 2019). This study used the station-based index of Hurrell (2015) which provides empirical evidence until 1864. This record is extended back to 1768, with two proxy-based reconstructions selected for their robustness against this instrumental data (Luterbacher et al., 2001; DJFM index, accessed from https://www.ncdc.noaa.gov/paleo-search/study/6275) and their novelty (Ortega et al., 2015; DFJ index, accessed from https://www.ncdc.noaa.gov/paleo-search/study/18935). In the following, these indices are either showed in their cumulative form or as decadal averages. To highlight the dominance of either the negative or positive phase of the NAO in winter, cumulative indices were computed. After Mazzarella and Scafetta (2012), the cumulative value of each index for a given year is taken as the inclusive sum of values for all previous years. Then over the 20th century onward, more frequent spit-end positions are compared to the station-based index, averaged over the 10 years preceding each observation. This averaging procedure was needed because of the irregularly sampled observations; the10-year window was found to fit well with this irregular resolution and the inertia of the system compared to the high interannual variability of the NAO (Hurrell, 1995).

Results and basis for discussion

Three periods of spit lengthening

Upper panel in Figure 8 represents the path of the Cap Ferret spit-end from 1768 to 2014; lower panels show cumulated NAO indices. The spit-end path reveals 3 periods over which the spit has dominantly grown across the inlet. These periods, over 40 years each, are delimited by local extrema of the spit-end position, on maps and photos of

1768-1826, 1865-1909 and 1932-1972. The 1st and 3rd periods are found when the negative phase of the NAO has dominated (Figure 8, lower panels). Likewise, according to the station-based index (Hurrell, 2015), the negative phase of the NAO has dominated during most of the 2nd period, until 1902, or 7 years before the map of 1909.

The Dalton Minimum

The 1st period of spit lengthening, characterized by a 3.5 km lengthening of the spit between 1805 and 1826, was also contemporaneous with the Dalton Minimum (DM, 1780-1830) climate anomaly. Figure 9 details this record lengthening and the subsequent retreat. The spit has grown while the tidal inlet had 2 well defined channels. Both northern and southern channels were preserved as the spit grew, but the inlet minimal width was divided by 3 in 1826 compared to that of 1768. Then between 1826 and 1865, the spit has retreated while the inlet width regained a width comparable to its 1768 level. In 1865 the southern channel was buried by the main inlet shoal that have steadily migrated southward since 1768 attached to the inlet's southern margin. Therefore, during a century, the spit has advanced against a double channelled inlet and has retreated when the inlet's southern channel closed. In terms of climate, this century encompassed the Dalton Minimum which was a period of anomalous coldness (van der Schrier and Barkmeijer (2005) and references therein).

DM is explained as a conjunction of low solar activity and major volcanic eruptions and has culminated in Europe with "the year without a summer" in 1816 (van der Schrier and Barkmeijer, 2005). Using a global circulation model, van der Schrier and Barkmeijer (2005) have pointed out the "higher occurrence probability at the European mid-

latitudes of the strongest cyclone under DM atmospheric conditions". Their results recall those from Shindell (2001) and Ineson et al. (2011), who showed that periods, or years, with low solar activity produce NAO negative like atmospheric configurations. Indeed, during the negative phase of the NAO low pressure systems are deviated southward (Hurrell and Deser, 2009). Furthermore, there is converging evidence of enhanced mid-latitude storminess during such cold periods, as recorded by the dune fields north and south of Cap Ferret (Clarke et al., 2002).

The dominance of the negative phase of the NAO during DM is also suggested by the cumulative NAO winter-index of Luterbacher et al. (2001), that decreased until 1830 (Figure 8, mid panel). However, as recalled by Poirier et al. (2017), NAO reconstruction tend to diverge in this period. For instance, the data from Ortega et al. (2015) only confirm Luterbacher's data until 1810 when, according to the more recent reconstruction, the positive phase begins to dominate again. On the other hand, when compared to the station-based index computed by (Hurrell, 2015) from the instrumental record, Luterbacher's reconstruction performs better. Indeed, Luterbacher's (DJFM) reconstruction is well correlated with the station-based index from 1864 onward (Figure 8 mid panel), while the correlation between Ortega's (DJF) reconstruction and instrumental data between 1864 and 1969 is weaker (Figure 8 lower panel); Pearson linear correlation coefficient (r) equal to 0.89 (p-value < 10^{-47}) in the first case, against a correlation coefficient of 0.47 (p-value < 10^{-6}) in the second case.

Correlation with NAO winter-indices

After the DM, the other 2 periods of spit growth happened while the negative phase of the NAO have dominated in winter, as supported by Hurrell's (2015) station-based index (Figure 8, middle panel). By opposition, periods of spit retreat systematically took place in periods dominated by the positive phase of the winter NAO; on Figure 8, periods delimited by the local extrema of the spit-end position, on maps and photos of 1826-1865, 1909-1932 and 1972-2014.

Over the 20th century, sharp movements of the spit-end like those around 1915 and 1972 were also synchronous with remarkable shifts of the NAO (Figure 10, upper panel): between 1909 and 2000, the spit-end path is significantly correlated with the decadal average of the NAO winter-index (r = -0.67, p-value < 10^{-4}).

Locally, the positive phase of NAO is known to produce higher and more oblique (clockwise shift) winter waves (Charles et al., 2012). The hindcast used in this study agrees with this and further shows how decadal averages of the winter NAO index and the alongshore wave power are well correlated (Figure 10, lower panel; r = 0.86, p-value < 10^{-16}). Correlation is greater than for the total wave power (WP), which has a correlation coefficient of 0.76 (p-value < 10^{-11}). This highlights the impact of the NAO on the local wave direction as well. Consequently, according to wave climate between 1949 and 2014, decades dominated by the positive phase of the NAO may produce an average alongshore wave power up to 30% greater than when the negative phase dominates (figure 10, lower panel).

Nonetheless, although winter wave power and NAO index remain correlated until 2014, their apparent relationship with the spit-end track is less clear at the beginning of the

21st century. Since 2000, averaged wave power and NAO index have regained a more neutral value while the spit have continued to retreat.

Sea level and inlet width variations

The ongoing erosion and retreat of the spit-end comes after the last significant lengthening which has culminated in 1972 (Figures 4 & 10). In addition to a dominant negative phase of the NAO in winter (Figures 8 & 10), the spit has then advanced across the inlet while, since the 1930s, sea level was rising at a relative slow pace (1.26 $mm.y^{-1}$) compared to that of the beginning and end of the 20th century (above 2.4 $mm.y^{-1}$; see Table 2 and Figure 6 lower panel). During this period, the inlet channel volume and the morphological amplitude of the inlet throat were also relatively stable or slightly decreased (Figure 5).

Around 1972, the spit-end growth was sharply interrupted. In the same time the morphological amplitude of the inlet throat remained stable until 1979. Instead, as the winter NAO abruptly shifts towards the dominance of the positive phase, the decadal averaged of the alongshore wave power increased and reached its highest level between 1970 and 1990. It is only after 1979 that the inlet channel volume has begun to increase, synchronous with an acceleration of sea level rise (Figure 6). Since then channel volume has increased over 25%, while the wave energy remains at an average level.

The increase in channel volume recalls the dramatic expansion of the inlet observed after 1826 (Figure 9). This first *breathing* then occurred as sea level has successively fallen and risen (Table 2). In the absence of detailed analysis of the evolution of the

inlet's dimensions over the second period of spit lengthening, linear trends presented in Table 2 reveal that for all 3 periods of spit lengthening, sea level has either fallen or has risen slower than during preceding and following periods.

Discussion

The auto-cyclic hypothesis

From the 1960s to until recently (2014), the present set of maps and photos has been gathered and analysed numerous times by several authors, mainly for engineering purposes (see Nahon, 2018, for references). The main idea which raised is that Cap Ferret's spit-end north-south oscillations could be an auto-cyclic response to the apparent cyclicity of the inlet channel configuration (with one or two channels). Michel and Howa (1997) detailed the cyclical nature of the inlet channels and conceptualized its impacts on the inlet's northern and southern margins. Among other impacts, their conceptual model predicts that the Cap Ferret spit extends southward when a single channel exists and by opposition retreats when two channels split the inlet. This feedback interaction was derived from approximately the same cartographic data presented in here. However, such hypothesis is far less than evident during over a third of the data coverage. Indeed, as shown in Figure 9, let's recall here that between 1769 and 1825, the spit has elongated while the inlet had two channels and that from 1825 to 1865, the spit has retreated when the southern channel was progressively buried. On the other hand, there is an apparent relationship between the spit-end behaviour and the North Atlantic climate over the entire study period.

Wave climate influence

Links between the NAO and the local wave climate could be part of the explanation to the spit – climate apparent relationship. Indeed, it appears that the spit grows across the inlet when NAO-negative ocean waves are more shore normal and/or the alongshore

wave power is below average. By opposition, the spit-end retreats when the alongshore wave power is stronger than average, and as so when the wave-driven alongshore sediment transport (LST) is more intense. Aagaard et al. (2004) have observed a similar relationship along the western Danish coast in northern Europe. Based on wind data from the first and last 30 years of the 20th century, they have pointed out the contribution of increased wind-wave driven LST, to the updrift erosion of the spit-end towards the end of the century. More recently, Aagaard and Sørensen (2013) have suggested the increase of the LST surpasses all terms in the sediment *imbalanced* equation, including sea-level rise. Underlying physical processes are yet to be identified, however they could either lie within LST – inlet flow interactions (Bertin et al., 2009), or within wave orientation – spit-growth relationship (Ashton et al., 2016).

On the one hand, Bertin et al. (2009) have shown with a process-based morphodynamic model, that sediment retention within tidal inlets could increase when waves approach the coast at a lower angle of incidence; therefore when, to all other parameters equal, LST is reduced. Locally, this is quite meaningful because the nonlinear superimposition of the southward LST induced waves and tidal residuals increase alongshore gradients in sediment transport (Cayocca, 2001).

On the other hand, simulations with coastal evolution models (CEM) suggest that the sole relationships between spit growth and wave orientation may also be at play (Ashton et al., 2016): less oblique waves (and a decreased LST) leads to the erosion of the spit on the updrift side of the fulcrum point and to the lengthening of spit distal end (Figure 11a), whereas increasing the wave incidence and the LST induces sediment retention updrift of the fulcrum point while the spit-end loses sediment and retreats

(Figure 11b). This apparent oscillation of the sediment budget around the fulcrum point recalls the behaviour of the Cap Ferret between 1826 and 1865 (Figures 9 & 11c). These examples provide some insights on the physics underlying the apparent relationship between local geomorphology and local waves. Increased LST and more oblique waves during the positive phase of the NAO may well have forced the spit-end to retreat, while the spit can advance across the inlet when the negative phase of the NAO produce waves with a reduced angle of incidence and lower rates of LST.

From a regional perspective, this behaviour differs from that of the Arçay sandspit (less than 250 km north of Cap Ferret). Allard et al. (2008) first suggested the rhythmic growth of Arçay sandspit was boosted by LST, and Poirier et al. (2017) further put into evidence the hierarchical control of the NAO and the East Atlantic–West Russia pattern. In the case of Arçay, higher rates of LST during the positive phase of the NAO are found to be responsible for the enhanced spit growth. Here we found it is the opposite at Cap Ferret. Therefore, the attempt by Poirier et al. (2017) to, in a second time, associate both spits behaviour is questionable. The reason may be the important difference of their back-barrier lagoon dimensions, which in the case of Arçay is a lot smaller. In the case of Cap Ferret, the large lagoon of the Bay of Arcachon engenders a large tidal prism that has shaped large inlet shoals. Then, the repartition of wave-driven sediment inputs, between the spit and the shoals, become more complex (Hoan et al., 2011; Kraus, 2000; Larson et al., 2007). This is particularly true when relative sea levels are subject to rise, ultimately turning shoals into sediment sinks because their equilibrium volume increases with the larger value of tidal prism engendered by higher sea level (Walton, Jr. and Adams, 1976). Also, wave climate variations alone may not

fully explain inlet constrictions and expansions such as those observed during and after the Dalton Minimum (Figure 2c-d), or the ongoing inlet throat expansion since 1979 (Figure 5).

Sea level influence

A tidal inlet's cross-section increases with tidal prism (O'Brien, 1931) and, to a lower degree, decreases with wave energy (Jarrett, 1976; Nahon et al., 2012). Tidal prism variations could then have contributed to observed changes in inlet dimensions. For instance, in 1990s when the wave energy is maximal (Figure 10, lower panel), only an increase of the tidal prism could have caused the inlet to enlarge (Figure 5e). In addition, the magnitude of the inlet's narrowing and widening in the first half of the 19th century (Figure 9) suggests that changes in the tidal prism have certainly added to the effects of variations of the wave climate associated with the Dalton Minimum. Over the study period, the Bay of Arcachon's contours remained stable. Instead, variations of the sea level must have modulated tidal prism.

Tidal flats and salt marshes occupy about 75 % of the Bay of Arcachon (Féniès and Faugères, 1998; Nahon, 2018), so that the tidal prism is mostly controlled by the relative elevation of those. Due to low sediment input from freshwater streams, the sedimentation rate above these tidal flats is expected to respond, at most, with a temporal lag to changes in the rate of sea level variations (Kirwan and Murray, 2008). So that when sea level starts to increase or when sea level rise (SLR) accelerates, tidal flats' relative elevation decreases temporarily, leading to a greater tidal prism that ultimately forces the inlet to enlarge. On the contrary, inlets may narrow in response to falling sea level or stable to decelerating SLR.

Part of the explanation would also be related to the ongoing morphological evolution whole barrier system. Indeed, the large tidal flats of the lagoon and the relatively high tidal range promote the ebb dominance of the system (Fortunato and Oliveira, 2005; Friedrichs and Aubrey, 1988). The overall negative sediment budget of the lagoon between charts of 1865 and 2001 (Allard et al., 2009) confirmed this characteristic. Charts further revealed that sediment loss was due to headward erosion of its tidal channels which, according to process-based models, can be a response of an inlet – lagoon system to SLR (van Maanen et al., 2013). This similitude between simulated morphologies and the observed evolution of the lagoon, suggests the Bay of Arcachon is currently adapting to secular regional SLR (Jevrejeva et al., 2014). Van Maanen et al. (2013) numerical experiments further explain how, under progressive SLR, such systems can remain ebb-dominated and how the amount of exported sediment increases with the rate of SLR.

Therefore, multiple processes could explain how decadal to pluri-decadal variations in the rate of SLR (Jevrejeva et al., 2014), like those observed at Brest (Figure 6 and Table 2), must have impacted the inlet sediment budget, at temporal scales matching those of documented spit-end oscillations.

Other influences

In winter, the NAO also modifies effective rainfalls and wind regimes as well as sea level anomalies (Calafat et al., 2012). Locally, NAO-positive winters tends to be drier (Hurrell and Deser, 2009), so that freshwater inputs to the lagoon are expected to be further reduced. Therefore, it is very unlikely that the impact of the NAO on precipitation

could contribute to the observed inlet breathing and spit oscillation. However, the morphodynamic impact of positive sea level anomalies during NAO negative winters (Calafat et al., 2012) and how it may interact with longer term trends of SLR is an open question. As is the impact of the complex wind-induced circulation (Salles et al., 2015) on inlet morphodynamics. Nonetheless, these questions fall beyond the scope of the present work.

Synthesis

Despite these latter questions, a combination of processes exists that may well have contributed to the north-south oscillations of the spit-end observed on charts and aerial photographs, between 1768 and 2014.

Variations in the wave climate associated with North Atlantic atmospheric state, very likely modified sediment transport patterns near the spit-end; and trends in sea level variations have modulated inlet dimensions, ultimately forcing the spit-end to retreat when the inlet enlarged faster that it was migrating and allowing the spit-end to advance otherwise. These two drivers make it possible to explain the spit decays and growths over the entire study period and at the temporal scale resolved by that cartographic data. Identifying a dominant mechanism is tricky though.

On the one hand, since the turn of the 20th century, the spit has then been able to durably grow when the rate of SLR was moderate, as between 1930 and 1970. Otherwise, when sea level has risen faster, like before 1930 or since 1970, the spit-end has been unstable or has retreated. This indicates the existence of an upper limit to the rate of SLR (around 2 mm.y^{-1} according data in Table 2), above which spit growth is

annihilated. On the other hand, even though regional SLR remained moderate until the late 1970s, the intensification of the alongshore wave power alone have trigger the spit retreat in the early 1970s. The next step would then be to implement a numerical morphodynamic model to rigorously evaluate the respective and relative contribution of both forcing.

Finally, independently from the existence of a dominant mechanism, the exceptional evolution during the first half of the 19th century was certainly produced by in-phase destructive and constructive forces: from the spit point of view, it must have resulted from synchronous constructive forces, exacerbated by the Dalton Minimum, followed by synchronous destructive forces. This certainly agrees with the duality of wave climate and sea level relations in terms of geomorphological impacts. However, it does not answer the question of the interplay between these two drivers.

Conclusions

Detailed observations of the Cap Ferret spit-end over the last 250 years reveal geomorphological changes of a remarkable magnitude. Owing to the temporal coverage, it seems possible to explain the apparent cyclical nature of this dynamic by a combination of climatic shifts and sea-level variations, although without considering an eventual relationship between these two drivers.

First, all documented phases of spit growth were found during periods dominated by the negative phase of the North Atlantic Oscillation in winter. Inversely, the spit has retreated when the NAO shifted towards a positive-phase dominance. The relationship between NAO and local wave climate make the wave climate a good candidate to

explain this behaviour. During the positive phase of the NAO, higher ocean waves and/or clockwise shifts of the waves' mean direction accelerate alongshore sediment transport (LST), which, counter intuitively and like it has been observed and modelled elsewhere, contribute the updrift erosion of the spit-end.

In the second place, spit-end retreats and instabilities were also in phase with periods of rapid or accelerating sea-level rise SLR. Synchronous expansions of the adjacent inlet pointed at the impact of SLR on tidal prism. Indeed, enhanced tidal prism under accelerating SLR may well exacerbate the ongoing adaptation of the whole Bay of Arcachon to secular SLR, ultimately forcing the spit-end to retreat when the inlet enlarges faster than in migrates downdrift.

Locally, these findings advocate a dominance of allocyclic mechanisms over the autocyclic behaviour proposed by Michel and Howa (1997). Somehow this goes along with the results of Allard et al. (2008) and Poirier et al. (2017), although the opposed behaviour of Cap Ferret and Arçay spits regarding wave climate suggest that coastal barrier spits response to increased LST may differs regarding if SLR is or not turning spits' adjacent shoals into sediment sinks.

In a broader perspective, the present results further highlight the vulnerability to SLR of barrier-spit backed by large estuaries. Given this, they may also serve to detect coastal adjustments driven by climate change.

Acknowledgments

A.N. was funded under a BRGM PhD grant with the support of the *Région Aquitaine* council and the *Syndicat Intercommunal du Bassin d'Arcachon*. We kindly acknowledge

Xavier Bertin (*CNRS-Université de La Rochelle*), for providing us with the wave hindcast, as well as our office colleagues Anais Hoareau and Anne Fondin for digitizing the bathymetric charts before 2001. We are grateful to our colleagues Thomas Bulteau, Bruno Castelle and Gonéri Le Cozannet, and to Giovanni Coco from the University of Auckland for their constructive feedback on an earlier version of the manuscript. We also thank Jennifer Simeon from Pessac based GEOSAT for proof reading the manuscript's final version. The geomorphological data can be requested by contacting the first author or the *Observatoire de la Côte Aquitaine* (http://www.observatoire-cote-aquitaine.fr/).

References

Aagaard T, Nielsen J, Jensen SG, Friderichsen J. 2004. Longshore sediment transport and coastal erosion at Skallingen, Denmark. Geografisk Tidsskrift-Danish Journal of Geography **104** : 5–14. DOI: 10.1080/00167223.2004.10649499

Aagaard T, Sørensen P. 2013. Sea level rise and the sediment budget of an eroding barrier on the Danish North Sea coast. Journal of Coastal Research **65** : 434–439. DOI: 10.2112/SI65-074.1

Allard J, Bertin X, Chaumillon E, Pouget F. 2008. Sand spit rhythmic development: A potential record of wave climate variations? Arçay Spit, western coast of France. Marine Geology **253** : 107–131. DOI: 10.1016/j.margeo.2008.05.009

Allard J, Chaumillon E, Féniès H. 2009. A synthesis of morphological evolutions and Holocene stratigraphy of a wave-dominated estuary: The Arcachon lagoon, SW France. Continental Shelf Research **29** : 957–969. DOI: 10.1016/j.csr.2008.11.017

Ashton AD, Nienhuis J, Ells K. 2016. On a neck, on a spit: controls on the shape of free spits. Earth Surface Dynamics **4** : 193–210. DOI: 10.5194/esurf-4-193-2016

Aubié S, Tastet J-P. 2000. Coastal Erosion, Processes and Rates: An Historical Study of the Gironde Coastline, Southwestern France. Journal of Coastal Research **16** : 756–767.

Barnard PL, Allan J, Hansen JE, Kaminsky GM, Ruggiero P, Doria A. 2011. The impact of the 2009-10 El Niño Modoki on U.S. West Coast beaches. Geophysical Research Letters **38** : n/a-n/a. DOI: 10.1029/2011GL047707

Barnston AG, Livezey RE. 1987. Classification, Seasonality and Persistence of Low-Frequency Atmospheric Circulation Patterns. Monthly Weather Review **115** : 1083–1126. DOI: 10.1175/1520-0493(1987)115<1083:CSAPOL>2.0.CO;2

Bertin X, Fortunato AB, Oliveira A. 2009. A modeling-based analysis of processes driving wave-dominated inlets. Continental Shelf Research **29** : 819–834. DOI: 10.1016/j.csr.2008.12.019

Bertin X, Li K, Roland A, Bidlot J-R. 2015. The contribution of short-waves in storm surges: Two case studies in the Bay of Biscay. Continental Shelf Research **96** : 1–15. DOI: 10.1016/j.csr.2015.01.005

Bruneau N, Fortunato AB, Dodet G, Freire P, Oliveira A, Bertin X. 2011. Future evolution of a tidal inlet due to changes in wave climate, Sea level and lagoon morphology (Óbidos lagoon, Portugal). Continental Shelf Research **31** : 1915–1930. DOI: 10.1016/j.csr.2011.09.001

Bruun P. 1978. Stability of Coastal Inlets: Theory and Engineering . Elsevier. [online] Available from: http://www.sciencedirect.com/science/bookseries/01651250/23

Calafat FM, Chambers DP, Tsimplis MN. 2012. Mechanisms of decadal sea level variability in the eastern North Atlantic and the Mediterranean Sea. Journal of Geophysical Research: Oceans **117** : n/a-n/a. DOI: 10.1029/2012JC008285

Caspari E. 1872. Rapport sur l'exploration des Passes du Bassin d'Arcachon

Castelle B, Guillot B, Marieu V, Chaumillon E, Hanquiez V, Bujan S, Poppeschi C. 2018. Spatial and temporal patterns of shoreline change of a 280-km high-energy disrupted sandy coast from 1950 to 2014: SW France. Estuarine, Coastal and Shelf Science **200** : 212–223. DOI: 10.1016/j.ecss.2017.11.005

Cayocca F. 2001. Long-term morphological modeling of a tidal inlet: the Arcachon Basin, France. Coastal Engineering **42** : 115–142. DOI: 10.1016/S0378-3839(00)00053-3

Cazenave A, Le Cozannet G. 2014. Sea level rise and its coastal impacts. Earth's Future **2** : 15–34. DOI: 10.1002/2013EF000188

CETMEF. n.d. CANDHIS (03302) - Bouée Cap Ferret [online] Available from: http://candhis.cetmef.developpement-durable.gouv.fr/campagne/?idcampagne=b6d767d2f8ed5d21a44b0e5886680cb9 (Accessed 6 March 2017)

Charles E, Idier D, Thiébot J, Le Cozannet G, Pedreros R, Ardhuin F, Planton S. 2012. Present Wave Climate in the Bay of Biscay: Spatiotemporal Variability and Trends from 1958 to 2001. Journal of Climate **25** : 2020–2039. DOI: 10.1175/JCLI-D-11-00086.1

Chowdhury P, Behera MR. 2017. Effect of long-term wave climate variability on longshore sediment transport along regional coastlines. Progress in Oceanography **156** : 145–153. DOI: 10.1016/j.pocean.2017.06.001

Clarke M, Rendell H, Tastet J-P, Clavé B, Massé L. 2002. Late-Holocene sand invasion and North Atlantic storminess along the Aquitaine Coast, southwest France. The Holocene **12** : 231–238. DOI: 10.1191/0959683602hl539rr

Clemmensen LB, Richardt N, Anderson C. 2001. Holocene sea-level variation and spit development: data from Skagen Odde, Denmark. The Holocene **11** : 323–331. DOI: 10.1191/095968301667877044

Cook ER, D'Arrigo RD, Mann ME. 2002. A Well-Verified, Multiproxy Reconstruction of the Winter North Atlantic Oscillation Index since a.d. 1400. Journal of Climate **15** : 1754–1764. DOI: 10.1175/1520-0442(2002)015<1754:AWVMRO>2.0.CO;2

Davis RA. 2013. Evolution of Coastal Landforms. In Treatise on Geomorphology , . Elsevier; 417–448. [online] Available from: http://linkinghub.elsevier.com/retrieve/pii/B9780123747396002931 (Accessed 20 April 2016)

Dissanayake DMPK, Ranasinghe R, Roelvink JA. 2012. The morphological response of large tidal inlet/basin systems to relative sea level rise. Climatic Change **113** : 253–276. DOI: 10.1007/s10584-012-0402-z

Dodet G, Bertin X, Taborda R. 2010. Wave climate variability in the North-East Atlantic Ocean over the last six decades. Ocean Modelling **31** : 120–131. DOI: 10.1016/j.ocemod.2009.10.010

Féniès H, Faugères J-C. 1998. Facies and geometry of tidal channel-fill deposits (Arcachon Lagoon, SW France). Marine Geology **150** : 131–148. DOI: 10.1016/S0025-3227(98)00049-8

Féniès H, Lericolais G. 2005. Internal architecture of an incised valley-fill on a wave- and tide-dominated coast (the Leyre incised valley, Bay of Biscaye, France). Comptes Rendus Geoscience **337** : 1257–1266. DOI: 10.1016/j.crte.2005.06.005

Féniès H, Lericolais G, Posamentier HW. 2010. Comparison of wave-and tide-dominated incised valleys: specific processes controlling systems tract architecture and reservoir geometry. Bulletin de la Societe Geologique de France **181** : 171–181. DOI: 10.2113/gssgfbull.181.2.171

FitzGerald D, Georgiou I, Miner M. 2015. Estuaries and Tidal Inlets. In Coastal Environments and Global Change , Masselink G and Gehrels R (eds). John Wiley & Sons, Ltd: Chichester, UK; 268–298. [online] Available from: http://doi.wiley.com/10.1002/9781119117261.ch12 (Accessed 19 May 2016)

FitzGerald DM, Fenster MS, Argow BA, Buynevich IV. 2008. Coastal Impacts Due to Sea-Level Rise. Annual Review of Earth and Planetary Sciences **36** : 601–647. DOI: 10.1146/annurev.earth.35.031306.140139

FitzGerald DM, Kraus NC, Hands EB. 2001. Natural mechanisms of sediment bypassing at tidal inlets . U.S. Army Engineer Research and Development Center: Vicksburg, MS

Fortunato AB et al. 2014. Morphological evolution of an ephemeral tidal inlet from opening to closure: The Albufeira inlet, Portugal. Continental Shelf Research **73** : 49–63. DOI: 10.1016/j.csr.2013.11.005

Fortunato AB, Oliveira A. 2005. Influence of Intertidal Flats on Tidal Asymmetry. Journal of Coastal Research **215** : 1062–1067. DOI: 10.2112/03-0089.1

Friedrichs CT, Aubrey DG. 1988. Non-linear tidal distortion in shallow well-mixed estuaries: a synthesis. Estuarine, Coastal and Shelf Science **27** : 521–545. DOI: 10.1016/0272-7714(88)90082-0

Fruergaard M, Andersen TJ, Johannessen PN, Nielsen LH, Pejrup M. 2013. Major coastal impact induced by a 1000-year storm event. Scientific Reports **3** DOI: 10.1038/srep01051 [online] Available from: http://www.nature.com/articles/srep01051 (Accessed 11 April 2016)

Fruergaard M, Andersen TJ, Nielsen LH, Johannessen PN, Aagaard T, Pejrup M. 2015. High-resolution reconstruction of a coastal barrier system: impact of Holocene sea-level change. Sedimentology **62** : 928–969. DOI: 10.1111/sed.12167

Glueck MF, Stockton CW. 2001. Reconstruction of the North Atlantic Oscillation, 1429-1983. International Journal of Climatology **21** : 1453–1465. DOI: 10.1002/joc.684

Hayes MO. 1979. Barrier island morphology as a function of tidal and wave regime. In Barrier Islands, from the Gulf of St. Lawrence to the Gulf of Mexico , . Leatherman, S.; 1–27.

Hoan LX, Hanson H, Larson M, Kato S. 2011. A mathematical model of spit growth and barrier elongation: Application to Fire Island Inlet (USA) and Badreveln Spit (Sweden). Estuarine, Coastal and Shelf Science **93** : 468–477. DOI: 10.1016/j.ecss.2011.05.033

Holgate SJ, Matthews A, Woodworth PL, Rickards LJ, Tamisiea ME, Bradshaw E, Foden PR, Gordon KM, Jevrejeva S, Pugh J. 2013. New Data Systems and Products at the Permanent Service for Mean Sea Level. Journal of Coastal Research **288** : 493–504. DOI: 10.2112/JCOASTRES-D-12-00175.1

Hubbard DK, Oertel GF, Nummedal D. 1979. The Role of Waves and Tidal Currents in the Development of Tidal-inlet Sedimentary Structures and Sand Body Geometry: Examples from North Carolina, South Carolina, and Georgia. SEPM Journal of Sedimentary Research **Vol. 49** DOI: 10.1306/212F78B5-2B24-11D7-8648000102C1865D [online] Available from: http://jsedres.sepmonline.org/cgi/doi/10.1306/212F78B5-2B24-11D7-8648000102C1865D (Accessed 26 September 2016)

Hurrell JW. 1995. Decadal Trends in the North Atlantic Oscillation: Regional Temperatures and Precipitation. Science **269** : 676–679. DOI: 10.1126/science.269.5224.676

Hurrell JW. 2015. The Climate Data Guide: Hurrell North Atlantic Oscillation (NAO) Index (Station-based) [online] Available from: https://climatedataguide.ucar.edu/climate-data/hurrell-north-atlantic-oscillation-nao-index-pc-based (Accessed 14 August 2015)

Hurrell JW. 2019. The Climate Data Guide: Hurrell North Atlantic Oscillation (NAO) Index (PC-based) [online] Available from: https://climatedataguide.ucar.edu/climate-data/hurrell-north-atlantic-oscillation-nao-index-pc-based (Accessed 26 January 2019)

Hurrell JW, Deser C. 2009. North Atlantic climate variability: The role of the North Atlantic Oscillation. Journal of Marine Systems **78** : 28–41. DOI: 10.1016/j.jmarsys.2008.11.026

Idier D, Castelle B, Charles E, Mallet C. 2013. Longshore sediment flux hindcast: spatio-temporal variability along the SW Atlantic coast of France. Journal of Coastal Research **165** : 1785–1790. DOI: 10.2112/SI65-302.1

Ineson S, Scaife AA, Knight JR, Manners JC, Dunstone NJ, Gray LJ, Haigh JD. 2011. Solar forcing of winter climate variability in the Northern Hemisphere. Nature Geoscience **4** : 753–757. DOI: 10.1038/ngeo1282

Jarrett JT. 1976. Tidal Prism - Inlet Area Relationships . Army Engineer Waterways Experiment Station: Vicksburg MS [online] Available from: http://cirp.usace.army.mil/pubs/archive/GITI-Report_Number_3.pdf

Jevrejeva S, Moore JC, Grinsted A, Matthews AP, Spada G. 2014. Trends and acceleration in global and regional sea levels since 1807. Global and Planetary Change **113** : 11–22. DOI: 10.1016/j.gloplacha.2013.12.004

Jones PD, Jonsson T, Wheeler D. 1997. Extension to the North Atlantic oscillation using early instrumental pressure observations from Gibraltar and south-west Iceland. International Journal of Climatology **17** : 1433–1450. DOI: 10.1002/(SICI)1097-0088(19971115)17:13<1433::AID-JOC203>3.0.CO;2-P

Kalnay E et al. 1996. The NCEP/NCAR 40-Year Reanalysis Project. Bulletin of the American Meteorological Society **77** : 437–471. DOI: 10.1175/1520-0477(1996)077<0437:TNYRP>2.0.CO;2

Kirwan ML, Murray AB. 2008. Tidal marshes as disequilibrium landscapes? Lags between morphology and Holocene sea level change. Geophysical Research Letters **35** DOI: 10.1029/2008GL036050 [online] Available from: http://doi.wiley.com/10.1029/2008GL036050 (Accessed 19 April 2016)

Kraus NC. 1998. Inlet Cross-Sectional Area Calculated by Process-Based Model. presented at the Conference on Coastal Engineering. Copenhagen, Denmark. 3265–3278 pp. [online] Available from: https://icce-ojs-tamu.tdl.org/icce/index.php/icce/article/view/5839 (Accessed 28 September 2016)

Kraus NC. 2000. Reservoir Model of Ebb-Tidal Shoal Evolution and Sand Bypassing. Journal of Waterway, Port, Coastal, and Ocean Engineering **126** : 305–313. DOI: 10.1061/(ASCE)0733-950X(2000)126:6(305)

Kraus NC, Seabergh WC. 2002. Inlet spits and maintenance of navigation channels . U.S. Army Engineer Research and Development Center: Vicksburg, MS [online] Available from: http://acwc.sdp.sirsi.net/client/search/asset/1000403 (Accessed 13 June 2016)

Lapeyre. 1925. Cartes du Pays de Buch, 1318 à 1913

Larson M, Kraus NC, Connell KJ. 2007. MODELING SEDIMENT STORAGE AND TRANSFER FOR SIMULATING REGIONAL COASTAL EVOLUTION. presented at the Proceedings of the 30th International Conference. San Diego, California, USA. 3924–3936 pp. April [online] Available from: http://www.worldscientific.com/doi/abs/10.1142/9789812709554_0330 (Accessed 22 March 2019)

Luterbacher J et al. 2001. Extending North Atlantic oscillation reconstructions back to 1500. Atmospheric Science Letters **2** : 114–124. DOI: 10.1006/asle.2002.0047

Luterbacher J, Schmutz C, Gyalistras D, Xoplaki E, Wanner H. 1999. Reconstruction of monthly NAO and EU indices back to AD 1675. Geophysical Research Letters **26** : 2745–2748. DOI: 10.1029/1999GL900576

van Maanen B, Coco G, Bryan KR, Friedrichs CT. 2013. Modeling the morphodynamic response of tidal embayments to sea-level rise. Ocean Dynamics **63** : 1249–1262. DOI: 10.1007/s10236-013-0649-6

Masselink G, Austin M, Scott T, Poate T, Russell P. 2014. Role of wave forcing, storms and NAO in outer bar dynamics on a high-energy, macro-tidal beach. Geomorphology **226** : 76–93. DOI: 10.1016/j.geomorph.2014.07.025

Masselink G, Castelle B, Scott T, Dodet G, Suanez S, Jackson D, Floc'h F. 2016. Extreme wave activity during 2013/2014 winter and morphological impacts along the Atlantic coast of Europe. Geophysical Research Letters **43** : 2135–2143. DOI: 10.1002/2015GL067492

Mazzarella A, Scafetta N. 2012. Evidences for a quasi 60-year North Atlantic Oscillation since 1700 and its meaning for global climate change. Theoretical and Applied Climatology **107** : 599–609. DOI: 10.1007/s00704-011-0499-4

Michel D, Howa HL. 1997. Morphodynamic behaviour of a tidal inlet system in a mixed-energy environment. Physics and Chemistry of the Earth **22** : 339–343. DOI: 10.1016/S0079-1946(97)00155-9

Nahon A. 2018. Ongoing morphological evolution of a Holocene coastal barrier-spit - The Cap Ferret, bounded by the Bay of Arcachon tidal inlet, PhD Thesis, University of Bordeaux: Bordeaux, France, October

Nahon A, Bertin X, Fortunato AB, Oliveira A. 2012. Process-based 2DH morphodynamic modeling of tidal inlets: A comparison with empirical classifications and theories. Marine Geology **291–294** : 1–11. DOI: 10.1016/j.margeo.2011.10.001

Nahon A, Idier D, Fenies H, Mugica J, Senechal N, Mallet C. 2015. Role of north atlantic climate variability on barrier-spit oscillations: the Cap Ferret. presented at the Coastal Sediments 2015. San Diego. July [online] Available from: http://www.worldscientific.com/doi/abs/10.1142/9789814689977_0240 (Accessed 21 April 2016)

Newton A et al. 2014. An overview of ecological status, vulnerability and future perspectives of European large shallow, semi-enclosed coastal systems, lagoons and transitional waters. Estuarine, Coastal and Shelf Science **140** : 95–122. DOI: 10.1016/j.ecss.2013.05.023

Nichols M, Allen G. 1981. Sedimentary processes in coastal lagoons. Unesco Technical Papers In Marine Science : 27–80.

O'Brien MP. 1931. Estuary tidal prisms related to entrance areas. Civil Engineering **1** : 738–739.

Ortega P, Lehner F, Swingedouw D, Masson-Delmotte V, Raible CC, Casado M, Yiou P. 2015. A model-tested North Atlantic Oscillation reconstruction for the past millennium. Nature **523** : 71–74.

PAB. 1985. Etude de l'évolution du littoral de la presqu'île du Cap Ferret . Port Autonome de Bordeaux, Direction de l'aménagement et de l'environnement maritimes: Bordeaux, France

Plus M, Dumas F, Stanisière J-Y, Maurer D. 2009. Hydrodynamic characterization of the Arcachon Bay, using model-derived descriptors. Continental Shelf Research **29** : 1008–1013. DOI: 10.1016/j.csr.2008.12.016

Poirier C, Tessier B, Chaumillon É, Bertin X, Fruergaard M, Mouazé D, Noël S, Weill P, Wöppelmann G. 2017. Decadal changes in North Atlantic atmospheric circulation patterns recorded by sand spits since 1800CE. Geomorphology **281** : 1–12. DOI: 10.1016/j.geomorph.2016.12.028

Ranasinghe R, Duong TM, Uhlenbrook S, Roelvink D, Stive M. 2012. Climate-change impact assessment for inlet-interrupted coastlines. Nature Climate Change **3** : 83–87. DOI: 10.1038/nclimate1664

Ridderinkhof W, Hoekstra P, van der Vegt M, de Swart HE. 2016. Cyclic behavior of sandy shoals on the ebb-tidal deltas of the Wadden Sea. Continental Shelf Research **115** : 14–26. DOI: 10.1016/j.csr.2015.12.014

Roland A, Zhang YJ, Wang HV, Meng Y, Teng Y-C, Maderich V, Brovchenko I, Dutour-Sikiric M, Zanke U. 2012. A fully coupled 3D wave-current interaction model on unstructured grids. Journal of Geophysical Research: Oceans **117** : n/a-n/a. DOI: 10.1029/2012JC007952

Salles P, Valle-Levinson A, Sottolichio A, Senechal N. 2015. Wind-driven modifications to the residual circulation in an ebb-tidal delta: Arcachon Lagoon, Southwestern France. Journal of Geophysical Research: Oceans **120** : 728–740. DOI: 10.1002/2014JC010311

van der Schrier G, Barkmeijer J. 2005. Bjerknes' hypothesis on the coldness during AD 1790–1820 revisited. Climate Dynamics **25** : 537–553. DOI: 10.1007/s00382-005-0053-0

Semedo A, Weisse R, Behrens A, Sterl A, Bengtsson L, Günther H. 2013. Projection of Global Wave Climate Change toward the End of the Twenty-First Century. Journal of Climate **26** : 8269–8288. DOI: 10.1175/JCLI-D-12-00658.1

Senechal N, Sottolichio A, Bertrand F, Goeldner-Gianella L, Garlan T. 2013. Observations of waves' impact on currents in a mixed-energy tidal inlet: Arcachon on the southern French Atlantic coast. Journal of Coastal Research **165** : 2053–2058. DOI: 10.2112/SI65-347.1

Shindell DT. 2001. Solar Forcing of Regional Climate Change During the Maunder Minimum. Science **294** : 2149–2152. DOI: 10.1126/science.1064363

Splinter KD, Davidson MA, Golshani A, Tomlinson R. 2012. Climate controls on longshore sediment transport. Continental Shelf Research **48** : 146–156. DOI: 10.1016/j.csr.2012.07.018

Svendsen IA. 2006. Linear Waves. In Introduction to Nearshore Hydrodynamics , . World Scientific; 49–205. [online] Available from: https://books.google.fr/books?id=g7-PHmnrvQcC

Walton, Jr. TL, Adams WD. 1976. Capacity of inlet outer bars to store sand. In Proceedings of the 15th Coastal Engineering Conference, Honolulu, HI , . ASCE; 1919–1937. [online] Available from: https://icce-ojs-tamu.tdl.org/icce/index.php/icce/article/viewFile/3161/2825

van der Wegen M. 2013. Numerical modeling of the impact of sea level rise on tidal basin morphodynamics. Journal of Geophysical Research: Earth Surface **118** : 447–460. DOI: 10.1002/jgrf.20034

Wiggins M, Scott T, Masselink G, Russell P, Castelle B, Dodet G. 2017. THE ROLE OF MULTI-DECADAL CLIMATE VARIABILITY IN CONTROLLING COASTAL DYNAMICS: RE-INTERPRETATION OF THE 'LOST VILLAGE OF HALLSANDS''.' Helsingor, Denmark. June [online] Available from: https://hal.archives-ouvertes.fr/hal-01578356

Wong PP, Losada IJ, Gattuso J-P, Hinkel J, Khattabi A, McInnes KL, Saito Y, Sallenger A. 2014. Coastal systems and low-lying areas. In Climate Change 2014: Impacts, Adaptation, and Vulnerability. Part A: Global and Sectoral Aspects. Contribution of Working Group II to the Fifth Assessment Report of the Intergovernmental Panel of Climate Change , Field, C.B. et al. (eds). Cambridge, United Kingdom and New York, NY, USA; 361–409.

Wöppelmann G, Pouvreau N, Coulomb A, Simon B, Woodworth PL. 2008. Tide gauge datum continuity at Brest since 1711: France's longest sea-level record. Geophysical Research Letters **35** DOI: 10.1029/2008GL035783 [online] Available from: http://doi.wiley.com/10.1029/2008GL035783 (Accessed 2 June 2016)

Zhou Z, Coco G, Jiménez M, Olabarrieta M, van der Wegen M, Townend I. 2014. Morphodynamics of river-influenced back-barrier tidal basins: The role of landscape and hydrodynamic settings. Water Resources Research **50** : 9514–9535. DOI: 10.1002/2014WR015891

Tables

Table 1. Morphological parameters of the inlet throat between 1949 and 2014.

year	Channel volume (Mm^3)	Shoal volume (Mm^3)	Mean elevation (m NGF)	Morphological amplitude (Mm^3)
1949	32.14	59.48	-5.50	42.69
1969	30.02	54.20	-5.61	38.80
1979	30.02	43.21	-6.17	34.74
2001	33.93	61.41	-5.53	44.02
2014	38.62	60.58	-5.82	46.65
mean	32.53	55.78	-5.77	41.38

Table 2. Trends in Brest tidal gauge annual sea level data.

Periods	Linear trend, $mm.y^{-1}$	Spit behaviour
1807-1835	-1.08	extending
1826-1872	0.14	retreating
1865-1909	-0.33	extending
1900-1934	2.5	retreating
1932-1972	1.26	extending
1968-2015	2.42	retreating

Table 3. Comparison of hindcasted wave parameters and wave buoy observations.

Wave Field	BIAS (% of mean)	ERMS (% of mean)	Pearson Corr. coeff.
Hs	-1.16	43 cm	0.93
WP	-2.4	-	0.93
wDir	3.75° (0°)	-	-
WPx	-3.4 (1.7)	-	0.93 (0.93)
WPy	27.1 (1.7)	-	0.80 (0.81)

Figures

Figure 1 – Location maps. **a**) Bathymetry of the Bay of Biscay, bordering the SW coast of France; **b**) Gironde sandy coast, between the Gironde Estuary and the Bay of Arcachon, former estuary of the Leyre river and now a lagoon, semi-enclosed by the Cap Ferret sand spit (coordinates given in Lambert 93, in meters); **c**) Satellite Landsat 8 image of the Bay's tidal inlet in October 2014, showing the main geomorphological units and the red dotted line indicating the 2014 coastline of the Cap Ferret spit-end, on the inlet's updrift margin.

Figure 2 – Nautical charts. **a**) Ordnance survey map from 1888, black circled dots indicate control points used for georeferencing the map, red dashed line is the coastline measured by GPS on 2014 spring, red stars indicate the 3 reference locations used for georeferencing nautical charts; **b**-**e**) examples of nautical charts used to measure the spit-end positions, indicated by asterisk symbols for every given date; **f-g**) Satelite Landsat image of the Bay of Arcachon and its tidal inlet in October 2014.

Figure 3 – Measuring the spit's extension relative to the position of Cap Ferret's lighthouse. **Upper panels**: charts and coastlines from 1768 and 1826 and Satellite Landsat 8 image from October 2014, red dotted lines represent the 2014 coastline and the red stars indicate the lighthouse's position, white dashed lines materialize the axe onto which spit-end positions were orthogonally projected and

measured, the black sector in the right panel represents the spit-end migration range; **lower panel****:** the grey curve shows the spit-end path between 1768 and 1936, grey error bars stand for historical charts and the black ones for modern charts, asterisk symbol stand for spit-end positions in Figure 2**b-e**.

Figure 4 – Positions of the Cap Ferret spit-end measured on aerial photographs. **Upper panels**: series of aerial photographs of the spit-end, red dotted lines represent the 2014 coastline, black asterisk symbols materialize the spit-end positions for the given years, superimposed on photographs from 1934 and 1946 are the shorelines reproduced from charts of 1932 and 1936 respectively; **lower panel**: distance of the spit-end to lighthouse's position, black asterisk symbols correspond to those on the upper panel.

Figure 5 – Inlet throat bathymetric data. **a**) summer 2014 along transect soundings; **b**) interpolated bathymetry with the -7 m NGF contours (black lines); **c**) -7 m NGF contours superimposed onto October 2014 Landsat image; **d**) erosion (blue) – deposition (red) patterns over the 12.74 km^2 area covered by all 5 surveys between 1949 and 2014; **e-h**) channel volume (below -7 m NGF) , shoal volume (above -7 m NGF), overlapping area mean depth (m NGF) and inlet morphological amplitude over panel **d**'s area (**e**,**f** and **h** are in percent of averaged values for all 5 surveys).

Figure 6 – Brest tidal gauge Mean Sea Level (MSL) variation. **Upper panel**: annual MSL data from 1807 to 2015 recovered from the PMSL observatory (Holgate et al., 2013), black lines are the 11-year centred running mean of annual measurements and the thick dotted red line is the quadratic fit of all the data; **lower panel****:** same as above with data from 20th century onward fitted with a 5th order polynomial function.

Figure 7 – Local, 54 m water depth wave hindcast. **Upper panel**: 90-day running mean of the wave power (WP; linear wave theory approximation) 15 km offshore Cap Ferret, solid blue line are wind wave model (WWM-II, Roland et al., 2012) results with Bertin et al. (2015) setup, dotted black line are the wave buoy observations (CETMEF, n.d.) between April 2011 and May 2014, data is normalized using mean WP value over the hindcast period (1948-2014); **lower panel****:** same as above with the alongshore component of the wave power (WPy); r values are Pearson's linear correlation coefficients between plotted curves.

Figure 8 – Spit-end path and cumulated winter NAO indices between 1768 and 2014. **Upper panel**: the grey curve shows the distance from the spit-end to the Cap Ferret lighthouse as on Figures 3&4 (red dotted frame is for next Figure 8's zoom); **mid panel**: darker blue curve is the cumulated winter (DJFM) index of the NAO reconstruction of Luterbacher et al. (1999), lighter blue curve is the same but for (Hurrell's (2015) station-based (DJFM) index; **lower panel**: darker blue curve is the cumulated winter (DJF) index of the NAO reconstruction of Ortega et al. (2015),

lighter blue curve is the same but for Hurrell's (2015) station-based (DJFM) index; on all panels, orange shades indicate periods of spit elongation with the Dalton Minimum period in darker orange, r values are Pearson's linear correlation coefficients between plotted curves.

Figure 9 – Evolution of the spit-inlet system across the Dalton Minimum (1780 – 1830). Navigation charts from years 1768, 1813, 1826 and 1865; blue asterisks indicate the positions of the spit terminus at the respective dates; black arrows materialize the inlet minimal width; red and blue arrows materialize the position of respectively the northern and southern channels; the dotted black line depicts the migration of the main inlet shoal barycentre; common red stars, dotted white axis and dotted red line are the same as in Figures 2 and 3.

Figure 10 – NAO relationships with Cap Ferret's spit-end and local wave climate. **Upper panel**: in grey is the path of the spit-end, as the distance from the spit-end to the Cap Ferret lighthouse, as on Figures 3&4 and over since 1909, superimposed blue curve is Hurrell's (2015) station-based NAO winter index, averaged of 10 years preceding each observation; **lower panel**: same winter NAO index curve as above, along with hindcasted alongshore winter wave power (WPy), averaged in same fashion as the NAO index and normalized using mean WPy value over the hindcast period (1948-2014); on both panels, orange shades indicate periods of spit elongation, r values are Pearson's linear correlation coefficients between plotted curves

Figure 11 – Sandspit's morphological response to changes in mean wave direction. **a**) spit-end response to a decrease of the averaged wave angle of incidence, modelled by (and reproduced from) Ashton et al. (2016), dashed line represents initial shoreline and shaded area represents the spit-end contours after waves became more shore normal; **b**) same as panel **a**, but for an increase of the averaged wave angle of incidence, or after waves became more oblique; **c**) dashed line represents Cap Ferret spit-end in 1826, at the end of the Dalton Minimum, and shaded area represents the spit-end in 1865.

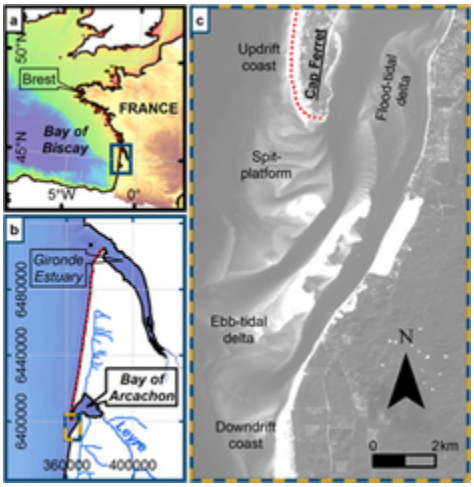

Location maps. **a**) Bathymetry of the Bay of Biscay, bordering the SW coast of France; **b**) Gironde sandy coast, between the Gironde Estuary and the Bay of Arcachon, former estuary of the Leyre river and now a lagoon, semi-enclosed by the Cap Ferret sand spit (coordinates given in Lambert 93, in meters); **c**) Satellite Landsat 8 image of the Bay's tidal inlet in October 2014, showing the main geomorphological units and the red dotted line indicating the 2014 coastline of the Cap Ferret spit-end, on the inlet's updrift margin.

19x20mm (300 x 300 DPI)

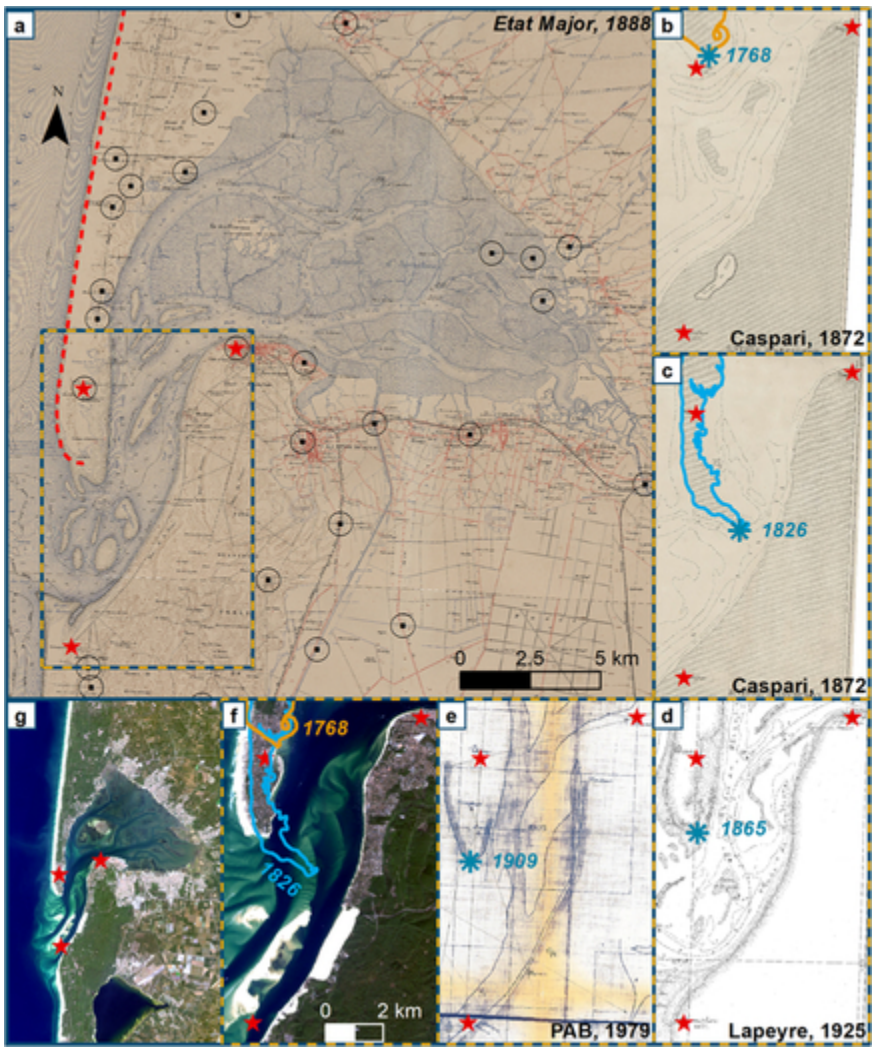

Nautical charts. **a**) Ordnance survey map from 1888, black circled dots indicate control points used for georeferencing the map, red dashed line is the coastline measured by GPS on 2014 spring, red stars indicate the 3 reference locations used for georeferencing nautical charts; **b-e**) examples of nautical charts used to measure the spit-end positions, indicated by asterisk symbols for every given date; **f-g**) Satelite Landsat image of the Bay of Arcachon and its tidal inlet in October 2014.

36x44mm (300 x 300 DPI)

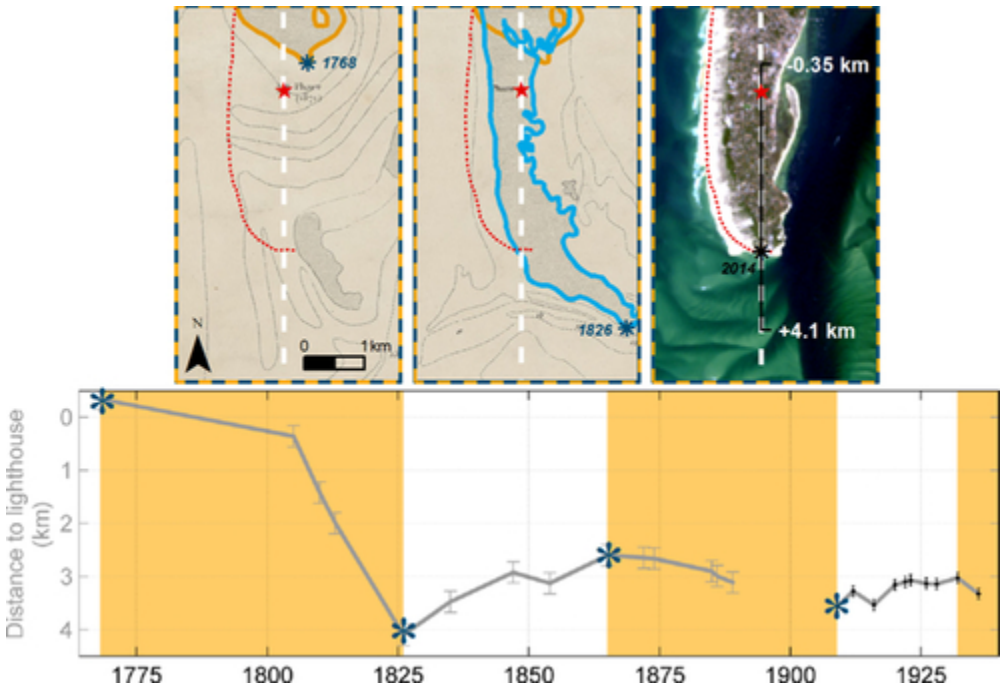

Measuring the spit's extension relative to the position of Cap Ferret's lighthouse. **Upper panels**: charts and coastlines from 1768 and 1826 and Satellite Landsat 8 image from October 2014, red dotted lines represent the 2014 coastline and the red stars indicate the lighthouse's position, white dashed lines materialize the axe onto which spit-end positions were orthogonally projected and measured, the black sector in the right panel represents the spit-end migration range; **lower panel**: the grey curve shows the spit-end path between 1768 and 1936, grey error bars stand for historical charts and the black ones for modern charts, asterisk symbol stand for spit-end positions in Figure 2**b-e**.

42x28mm (300 x 300 DPI)

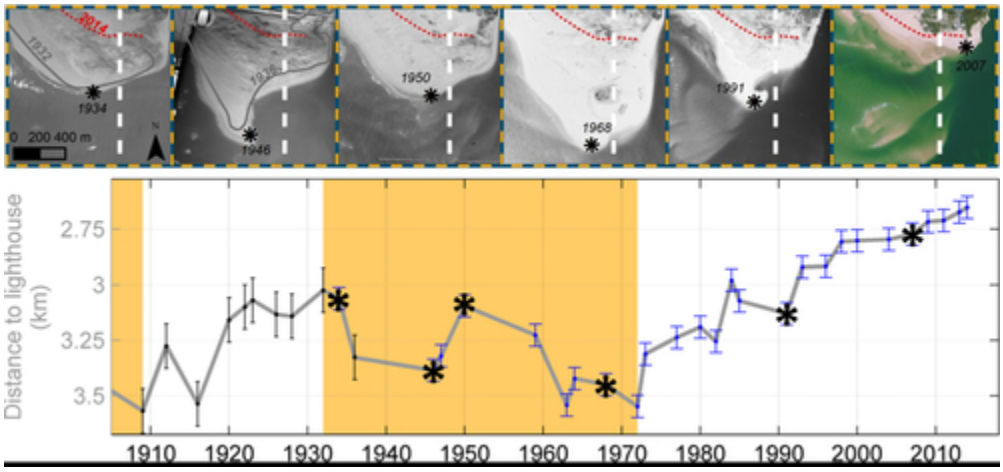

Positions of the Cap Ferret spit-end measured on aerial photographs. **Upper panels**: series of aerial photographs of the spit-end, red dotted lines represent the 2014 coastline, black asterisk symbols materialize the spit-end positions for the given years, superimposed on photographs from 1934 and 1946 are the shorelines reproduced from charts of 1932 and 1936 respectively; **lower panel**: distance of the spit-end to lighthouse's position, black asterisk symbols correspond to those on the upper panel.

42x19mm (300 x 300 DPI)

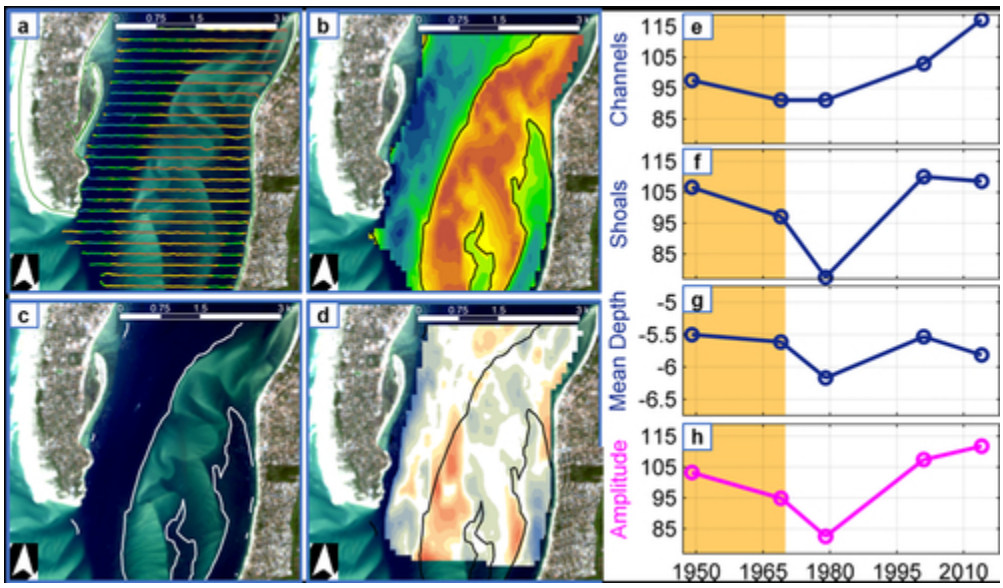

Inlet throat bathymetric data. **a**) summer 2014 along transect soundings; **b**) interpolated bathymetry with the -7 m NGF contours (black lines); **c**) -7 m NGF contours superimposed onto October 2014 Landsat image; **d**) erosion (blue) – deposition (red) patterns over the 12.74 km^2 area covered by all 5 surveys between 1949 and 2014; **e-h**) channel volume (below -7 m NGF) , shoal volume (above -7 m NGF), overlapping area mean depth (m NGF) and inlet morphological amplitude over panel **d**'s area (**e**,**f** and **h** are in percent of averaged values for all 5 surveys).

42x24mm (300 x 300 DPI)

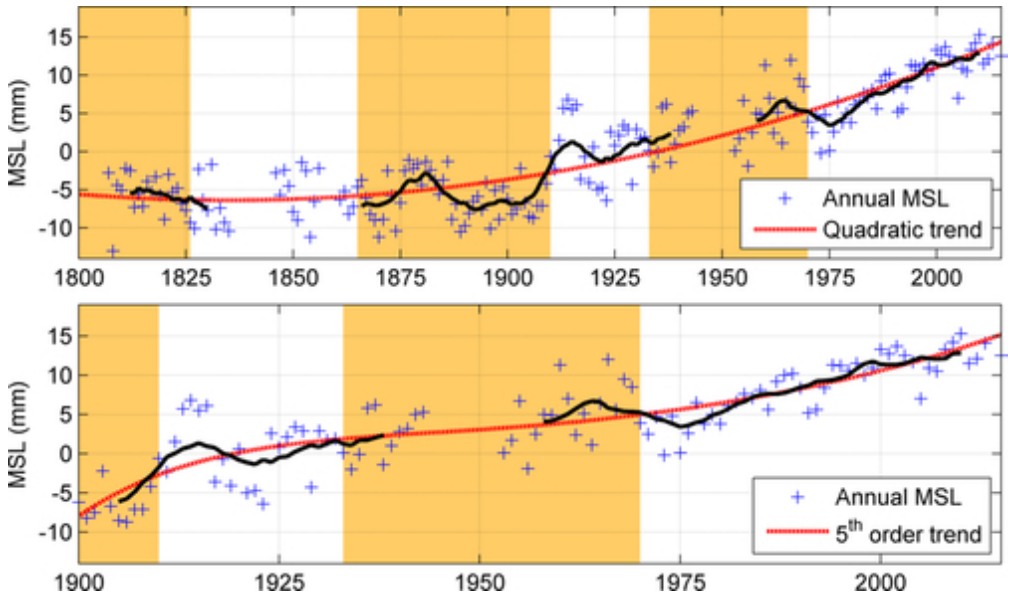

Brest tidal gauge Mean Sea Level (MSL) variation. **Upper panel**: annual MSL data from 1807 to 2015 recovered from the PMSL observatory (Holgate et al., 2013), black lines are the 11-year centred running mean of annual measurements and the thick dotted red line is the quadratic fit of all the data; **lower panel**: same as above with data from 20th century onward fitted with a 5th order polynomial function.

42x24mm (300 x 300 DPI)

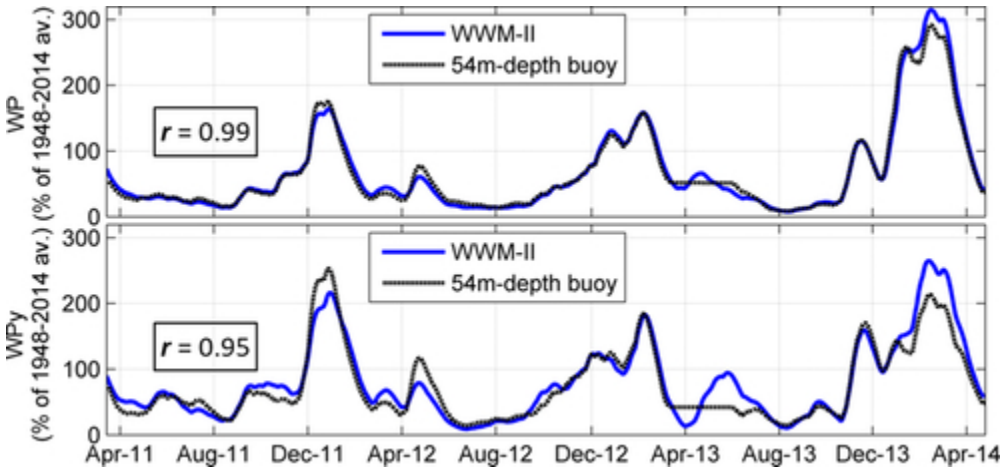

Local, 54 m water depth wave hindcast. **Upper panel**: 90-day running mean of the wave power (WP; linear wave theory approximation) 15 km offshore Cap Ferret, solid blue line are wind wave model (WWM-II, Roland et al., 2012) results with Bertin et al. (2015) setup, dotted black line are the wave buoy observations (CETMEF, n.d.) between April 2011 and May 2014, data is normalized using mean WP value over the hindcast period (1948-2014); **lower panel**: same as above with the alongshore component of the wave power (WPy); ***r*** values are Pearson's linear correlation coefficients between plotted curves.

42x19mm (300 x 300 DPI)

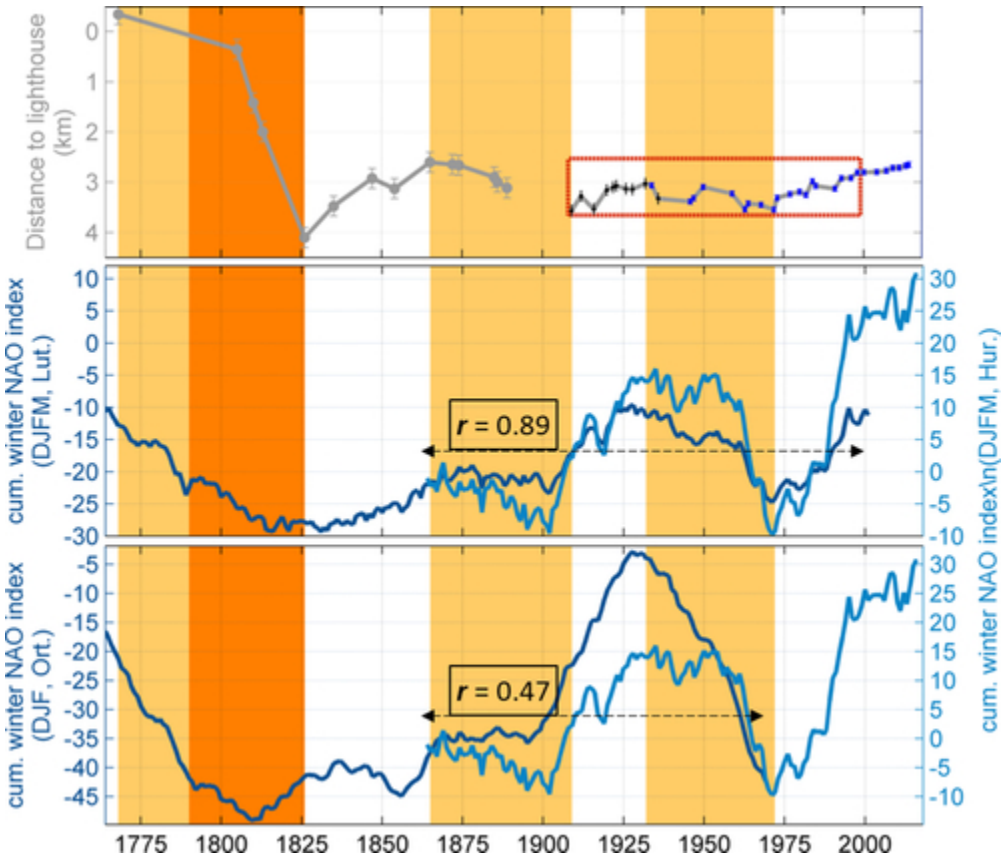

Spit-end path and cumulated winter NAO indices between 1768 and 2014. **Upper panel**: the grey curve shows the distance from the spit-end to the Cap Ferret lighthouse as on Figures 3&4 (red dotted frame is for next Figure 8's zoom); **mid panel**: darker blue curve is the cumulated winter (DJFM) index of the NAO reconstruction of Luterbacher et al. (1999), lighter blue curve is the same but for (Hurrell's (2015) station-based (DJFM) index; **lower panel**: darker blue curve is the cumulated winter (DJF) index of the NAO reconstruction of Ortega et al. (2015), lighter blue curve is the same but for Hurrell's (2015) station-based (DJFM) index; on all panels, orange shades indicate periods of spit elongation with the Dalton Minimum period in darker orange, ***r*** values are Pearson's linear correlation coefficients between plotted curves.

42x35mm (300 x 300 DPI)

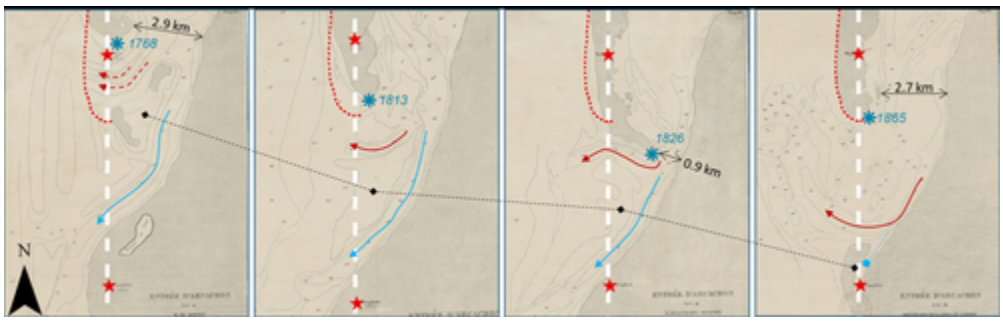

Evolution of the spit-inlet system across the Dalton Minimum (1780 – 1830). Navigation charts from years 1768, 1813, 1826 and 1865; blue asterisks indicate the positions of the spit terminus at the respective dates; black arrows materialize the inlet minimal width; red and blue arrows materialize the position of respectively the northern and southern channels; the dotted black line depicts the migration of the main inlet shoal barycentre; common red stars, dotted white axis and dotted red line are the same as in Figures 2 and 3.

42x13mm (300 x 300 DPI)

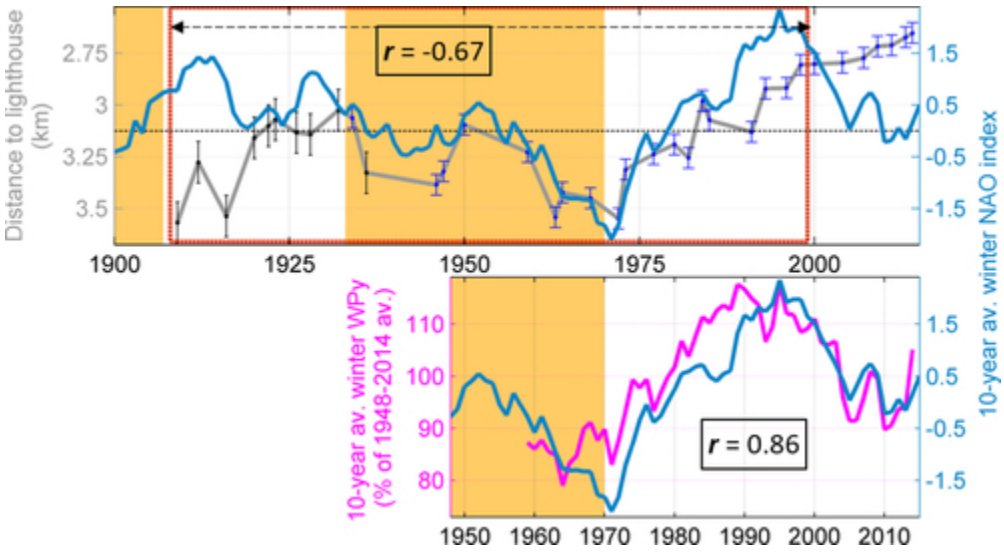

NAO relationships with Cap Ferret's spit-end and local wave climate. **Upper panel**: in grey is the path of the spit-end, as the distance from the spit-end to the Cap Ferret lighthouse, as on Figures 3&4 and over since 1909, superimposed blue curve is Hurrell's (2015) station-based NAO winter index, averaged of 10 years preceding each observation; **lower panel**: same winter NAO index curve as above, along with hindcasted alongshore winter wave power (WPy), averaged in same fashion as the NAO index and normalized using mean WPy value over the hindcast period (1948-2014); on both panels, orange shades indicate periods of spit elongation, ***r*** values are Pearson's linear correlation coefficients between plotted curves.

42x22mm (300 x 300 DPI)

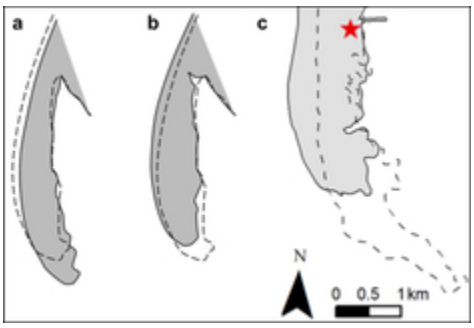

Sandspit's morphological response to changes in mean wave direction. **a**) spit-end response to a decrease of the averaged wave angle of incidence, modelled by (and reproduced from) Ashton et al. (2016), dashed line represents initial shoreline and shaded area represents the spit-end contours after waves became more shore normal; **b**) same as panel **a**, but for an increase of the averaged wave angle of incidence, or after waves became more oblique; **c**) dashed line represents Cap Ferret spit-end in 1826, at the end of the Dalton Minimum, and shaded area represents the spit-end in 1865.

19x13mm (300 x 300 DPI)